Whitlockite nanoparticle-coated hydroxyapatite granules for bone regeneration in defect of rat calvaria

Won-Bum Lee
Pusan National University College of Dentistry: Pusan National University School of Dentistry
Caifeng Wang
National Center for Nanoscience and Technology
Yoon-Seo Jang
Pusan National University College of Dentistry: Pusan National University School of Dentistry
Ki-Jae Jeong
Chungnam National University
Hyojin Kang
Chungnam National University
Ayun Seol
Pusan National University - Milyang Campus
Eun Seo Park
Pusan National University - Milyang Campus
Ho-Jin Lee
Chungnam National University School of Medicine
Dae Youn Hwang
Pusan National University - Milyang Campus
Jaebeom Lee (nanoleelab@gmail.com)
Chungnam National University
Dae-Seok Hwang
Pusan National University Dental Hospital

Research Article

Keywords: calvarial bone defect, whitlockite, WHHAGs, BMP and Wnt signaling pathways, bone regeneration

Posted Date: July 19th, 2023

DOI: https://doi.org/10.21203/rs.3.rs-3125669/v1

Abstract

Background

Whitlockite (WH; $Ca_{18}Mg_2(HPO_4)_2(PO_4)_{12}$) as the second most abundant ceramic of human bone after hydroxyapatite (HA; $Ca_{10}(PO_4)_6(OH)_2$), possessing high osteogenic activity, has been known that it can stimulate osteogenic differentiation as well as suppress osteoclastic activity, particularly, in the preparatory stage of bone regeneration.

Methods

In this work, we construct a unique ceramic structure by layering WH on the surface of HA granules (HAGs)s via dip-coating and sintering method.

Results

The cell proliferation of the WH-coated HAGs (WHHAGs) group in the cell counting kit (CCK-8) was about 1.15-fold higher than that of the NT group at 72 h after incubation. The western blot and qPCR results demonstrated that WHHAGs treatment readily stimulated the transcription of osteogenic genes by regulating the downstream signaling pathway of BMP and WNT receptors.This study presents a histological and radiological evaluation of the bone healing potential of the WHHAGs in a 7 mm diameter calvarial bone defect in rats, compared with/without the BMP and non-treated (NT) groups at the 8 weeks after surgery. The bone volume fraction (bone volume/tissue volume) of the WHHAGs group was about 7.32- and 3.56- fold higher than that of the NT group with/without the BMP, respectively. Besides, histological evaluation confirmed that the WHHAGs with BMP promoted bone regeneration.

Conclusion

These results suggest that the WHHAGs present the remarkable potential for application in dental and orthopedic bone regeneration.

1. Introduction

Maintenance of healthy alveolar bone is becoming more and more important with global aging[1]. The alveolar bone defect is often caused by extraction, severe periodontitis, trauma, and tumor resection, and it can affect nutritional deficiency as well as cognitive ability[2]. The resulting bone defect hinders implant-prosthetic rehabilitation and has an aesthetic adverse effect[3]. Bone graft materials used to regenerate alveolar bone in dentistry include autogenous bone, allograft, xenograft, and alloplastic materials. Although autogenous bone graft is considered as the golden standard for regenerating new

alveolar bone, the bone volume is limited, and donor site morbidity exists[4]. Allo- and xenograft materials may usually induce an immune reaction and corresponding transfer diseases, so alloplastic materials are often used to relieve donor site morbidity[5–7]. However, there are several alloplastic materials, including ceramics, polymers, and metals, calcium phosphates are recognized as suitable biomaterials that possess osteoconductive and osteoinductive characteristics, such as hydroxyapatite (HA; $Ca_{10}(PO_4)_6(OH)_2$), whitlockite (WH; $Ca_{18}Mg_2(HPO_4)_2(PO_4)_{12}$), tricalcium phosphate (*β*-TCP) [8–12]. HA occupies the most considerable portion of inorganic components in human bone[13]. Since HA does not induce inflammatory reaction and is typically osteoconductive, and can be directly combined with natural bone, it is artificially synthesized *in vitro* and used as a bone graft material[14, 15]. The purpose of bone grafting is ultimately to replace the transplant material with its own bone, but for externally synthesized HA, it remains almost undissolved *in vivo*, preventing complete replacement with self-bone. On the other hand, *β*-TCP is known as a substance that is not as biocompatible as HA, but is easily decomposed *in vivo*. When transplanted into a living body, it is gradually decomposed and replaced with regenerated bones, but it may be absorbed too quickly to support natural bones until they are sufficiently regenerated[16].

WH is found in various tissues of the human body that have not yet protruded, such as bone and cartilage, gallstones or decayed teeth, calculus, tuberculosis tissue, intervertebral discs, aorta, and teeth, and is widely distributed in normal and pathological tissue of the human body. Such WH is known as a material suitable for bone or teeth due to its structure or composition. In addition, the Ca/P ratio of WH is about 1.29:1, and it has a composition closer to the composition ratio of β-TCP, 1.5:1, than that of HA, 1.67:1, so WH has more similar properties to *β*-TCP than HA. It has been known that it may be more suitable for use in the restoration of human bone or tooth tissue when WH and HA are used in a certain amount. Conventionally, experiments for synthesizing WH have been conducted by various methods, but there have been considerable difficulties in obtaining it with high purity. As a result, the utilization of the WH was minimal.

There have been many attempts to produce mass-scale and pure WH. For example, Hong *et al.* proposed a method for mass production of nano-sized high-purity WH powders without a high-temperature thermal treatment and washing process[17]. However, with a scale-up process, obtaining high-purity nanoparticles (NPs) was difficult, and the amount of WH obtained from the process was very limited[18]. In particular, the macroporous structure of ceramic has been attractive because ceramics with a porous structure has a wider contact surface with the bloodstream than a dense structure when *in vivo* implantation, and new blood vessels and surrounding bone tissue can easily come to grow in and improve the fusion rate[19]. On the other hand, bone morphogenetic proteins (BMPs), one of the endogenous growth factors, play important roles in the regulation of differentiation of osteoprogenitor cells into osteoblasts[15, 20]. Among many BMP subtypes, BMP-2 and BMP-7 are the most potent osteoinductivity for bone regeneration[21, 22]. With the development of molecular cloning technology, human recombinant BMP (rhBMP) has been developed to control immune response properly[23]. To prevent its unexpected dispersion from the application site with the gradual release, a suitable carrier for BMP has been

developed. In particular, calcium phosphate has already been reported as an excellent BMP carrier[24–29]. BMP adsorption onto HA can improve the osteoconductive interaction of applied HA in the vicinity of a bone. Thereby more bone regeneration can be easily observed[30, 31]. However, it has been unexpectedly reported that alloplastic HA is poorly resorbed and may prevent rapid bone turnover in the bone graft site.[31] Whereas WH is a calcium phosphate-based ceramic that contains magnesium[32], [33]. Interestingly, compared to HA, WH showed greater compressive strength and higher resorbability, allowing higher ions to release BMPs steadily and continuously[34, 35]. Furthermore, magnesium ions released from WH may reduce osteoclast activity in the early stages of new bone formation and stimulate osteogenic differentiation[36, 37]. Therefore, bone turnover is expected to be improved using WH-coated HA granules (WHHAGs).

In the study, we announced a novel synthesis method of WH to be scalable where it can be produced in a high-purity, which is probably the first report to produce WH in a scalable system. Furthermore, a hybrid composite process of WH and HAGs was suggested to be applied to bone regeneration. Then, a fabrication process was introduced to produce WHHAGs through vacuum filtration as well as sintering treatment. The bone defect regeneration with the optimized WHHAGs with/without BMP-2 was carefully evaluated with a 7 mm diameter rat calvarial defect model using histological and radiographical evaluation.

2. Materials and methods

2.1. Materials

Chemicals, including calcium chloride ($CaCl_2$), magnesium chloride ($MgCl_2$), sodium phosphate dibasic (Na_2HPO_4), and poly(vinyl alcohol) (PVA), were purchased from Sigma-Aldrich (St. Louis, MO, USA). HAG ($Ca_{10}(PO_4)_6(OH)_2$, Bongros™) with a typical diameter of 1 ~ 2 mm was obtained from CGBIO Inc. (Korea).

2.2. Scalable synthesis of WH NPs

WHNPs in this study were synthesized with a wet precipitation method. In brief, the aqueous solutions of 0.1 M $CaCl_2$ and 0.1 M $MgCl_2$ were mixed well with a specific ratio under 500 rpm stirring. Next, 21 mL of 0.1 M Na_2HPO_4 was added to the above mixture. The ratio of Mg^{2+}, Ca^{2+}, and PO_4^{3-} was equal to 2:8:7. Subsequently, the reaction mixture temperature was increased to 70 ℃ and kept for 24 h. The obtained NPs were separated with centrifugation, washed with deionized water, and dried into powder at 60 ℃ for the following WHHAGs fabrication process.

2.3. Preparation of WHHAGs

The fabrication process of WHHAGs is shown in Scheme 1. Briefly, WH NPs were dispersed well in 5% PVA solution (FDA approved and biologically compatible) to be 20 mg/mL using the sonic treatment for 30 min. Then, HAGs with the size of 1–2 mm were immersed in the prepared WH solution and dried under

60°C for 3 h. Finally, the WH-coated HAGs were sintered at 700°C for 2h in a tube furnace to remove the polymer completely and enhance the bonding of the WH layer to HAGs to be WHHAGs.

2.4. Characterization of the synthesized WH NPs and WHHAGs

The morphology and structure of WH NPs were characterized using transmission electron microscopy (TEM; H-7600, Hitachi, Japan) and high-resolution TEM (HRTEM; FEI, Talos F200X; Thermo Scientific). An X-ray powder diffractometer (Empyrean series-2; PANalytical, Netherlands) of CNU Chemistry Core Facility using Cu Kα radiation was used to characterize the crystal phase. Fourier transform infrared spectroscopy (FTIR) was performed using PerkinElmer Spectrum Two (Perkin-Elmer, UK). Morphologies and structures of WHHAGs were characterized using field emission scanning electron microscopy (FE-SEM; Hitachi S-4800, Japan).

2.5. Cell cultures

MG63 cells isolated from the bone of patients with osteosarcoma, were obtained from the American Type Culture Collection (ATCC, Mannassas, VA, USA). They were cultured in Dulbecco Modified Eagle's Medium (DMEM, Welgene, Gyeongsan, Korea) supplemented with 10% fetal bovine serum (FBS, Welgene), 2 mM L-glutamine, 100 u/mL penicillin, and 100 μg/mL streptomycin (Thermo Scientific Inc., Waltham, MA, USA). These cells were incubated in a humidified incubator at 37°C in an air atmosphere containing 5% CO_2.

2.6. Cell proliferation and cell cycle assay

MG63 cells were seeded in 96 well plates (2×10^4 cells/well) and cultured for 24 h. Then, the WHHAGs were treated in new media at each concentration (NT, WHHAG0.1, WHHAG1, WHHAG10, WHHAG24, WHHAG50, which represent non-treated, 0.1, 1, 10, 25, and 50 μg/ml, respectively. After the incubation for 24, 48, and 72 h, cell viability reagent (CCK-8: Dojindo, Kumamoto, Japan) was added to each well to make a total of 10%, and a microplate reader (Sunrise Remote Control) was utilized to check cell proliferation after 4 h, and a microplate reader (Tecan, Austria) was used to measure the absorbance at 450 nm.

The cell cycle of MG63 cells was evaluated using a Muse™Cell Cycle Kit (MCH100106, Millipore Co., Billerica, MA, USA) according to the manufacturer's instructions. Briefly, MG63 cells were cultured in 100 mm^2 dishes (3×10^5 cells/dish), then treated with three different concentrations of WHHAGs (10, 25, and 50 μg/mL) for 72 h. Total cells from subset groups were harvested by centrifugation at 3,000× g for 5 min and fixed with 70% EtOH at 20°C for 3 h. The fixed cells were washed with 1× PBS and resuspended in 200 μL of cell cycle reagent. Following incubation at 37°C in a CO_2 incubator for 30 min, cell cycles were analyzed using fluorescence-activated cell sorting (FACS, Millipore Co.).

2.7. Alkaline phosphatase (ALP) staining

ALP is one essential enzyme for bone formation and the early indicator of osteogenic differentiation[38]. The osteogenic differentiation capacity of WHHAGs was evaluated by ALP staining. Briefly, MG63 cells were seeded in a 24 well plate at 3×10^4 cells/well, cultured for 24 h, and then differentiated by treatment with a differentiation medium (50 μg/ml ascorbic acid, 0.1 μM dexamethasone and 10 mM β-glycerophosphate) to induce differentiation. The WHHAGs were treated with the differentiation medium at a concentration of 50 ug/ml. The culture medium was replaced every 3 days. After 7 and 14 days, differentiation-induced cells were treated according to the manual using the ALP staining kit (Cell Biolabs, Inc., San Diego, USA). ALP activities were confirmed through the degree of cell staining observed directly using optical microscopy.

2.8. Western blot analysis

The expression levels of the lipid metabolism-related proteins were quantified with the Western blot assay as described elsewhere[39, 40]. The total proteins were extracted from MG63 cells using Pro-Prep Protein Extraction Solution (iNtRON Biotechnology, Seongnam, Korea) and quantified with SMARTTM BCA Protein Assay Kit (Thermo Scientific Inc.). An appropriate amount of protein (30 μg) was collected from total cell lysate, loaded equally, and separated by 4–20% sodium dodecyl sulfate–polyacrylamide gel electrophoresis (SDS-PAGE) for 2 h, after which the resolved proteins were transferred to nitrocellulose membranes at 40 V for 2 h. Each membrane was incubated overnight at 4°C with the primary antibodies, diluted in 1:1,000 (Table S1). The probed membranes were washed with a washing buffer (137 mM NaCl, 2.7 mM KCl, 10 mM Na_2HPO_4, and 0.05% Tween 20) and incubated with 1:2,000 diluted horseradish peroxidase (HRP)-conjugated goat anti-rabbit IgG (Invitrogen) at room temperature for 1 h. The membrane blots were developed using an Amersham ECL Select Western Blotting detection reagent (GE Healthcare, Little Chalfont, UK). The chemiluminescence signals originating from the specific bands were detected using FluorChemi®FC2 (Alpha Innotech Co., San Leandro, CA, USA).

2.9. Quantitative reverse transcription-polymerase chain reaction (RT-qPCR) analysis

The transcription levels of osteocalcin (OCN), ALP, runt-related transcription factor 2 (RUNX2), bone morphogenetic protein-2 (BMP2), type I collagen (Col-I), and Vascular endothelial growth factor (VEGF) genes were quantified by RT-qPCR. Briefly, the total RNA of the subset groups was extracted with RNAzol (Tel-Test Inc., Friendswood, TX, USA) from MG63 cells according to the manufacturer's guidelines. The total RNA molecules were quantified using a Nano-300 Micro-Spectrophotometer (Allsheng Instruments Co. Ltd., Hangzhou, China), and the complementary DNA was synthesized using a mixture of the total RNA (5 μg), oligo-dT primer (Invitrogen, Carlsbad, CA, USA), dNTP, and reverse transcriptase (Superscript II, Invitrogen) on a T100TM thermal cycler (Bio-Rad, Hercules, CA, US). Using the synthesized cDNA template, qPCR was conducted from 2× Power SYBR Green (Toyobo Co., Osaka, Japan) with the following cycles: 15 sec at 95°C, 30 sec at 55°C, and 60 sec at 70°C. The cDNA for OCN, ALP, RUNX2, BMP2, Col-I, and VEGF genes are amplified using the specific primer sequences (Table S2). In the exponential phase of PCR amplification, the reaction cycle in which the PCR product exceeds this

fluorescence intensity threshold is considered the threshold cycle (Ct). The expression of the target gene was quantified relative to that of the housekeeping gene β-actin, based on a comparison of the Ct values at a constant fluorescence intensity according to Livak and Schmittgen's method[41].

2.10. Animals and Surgical Procedure

A total of 28 male Wistar rats were purchased from SMATCO corporation (Osan, Korea) and used for this study. The rats used in this experiment were between 7 weeks of age and weighed 250–300 g, and were provided with free access to food and water through cages. All experimental procedures were performed according to the ethical guidelines of Pusan National University Institutional Animal Care and Use Committee (PNUIACUC, South Korea), which comply with the regulation of the International Association for Study of Pain (IASP) in animals. (PNU-2020-2616). The rats were divided into four groups: Group 1 is the negative control group (four rats, non-treated (NT) group), Group 2 is the reference control or bovine hydroxyapatite (Bio-Oss®, Geistlich Pharma AG, Wolhusen, Switzerland) group (eight rats, Bio-Oss group), Group 3 is the WH coated HAG group (eight rats, WHHAGs group) and Group 4 is the WHHAGs with rhBMP-2 (Cowell BMP, Cowell medi inc., Busan, Korea) group (eight rats, WHHAGs + BMP group).

The rats were anesthetized with an intraperitoneal injection of a ketamine/xylazine cocktail at the concentration of 100 mg/kg ketamine (Yuhan, Seoul, Korea) and 10 mg/kg xylazine (Rompun, BAYER KOREA Ltd., Seoul, Korea). To prevent infection, the surgical site was shaved with an electric shaver and disinfected with betadine (povidone-iodine) using sterile tools and gloves. Then, 0.3 mL of lidocaine solution (1:100,000 epinephrine) was injected subcutaneously into calvarial soft tissue as a local anesthetic agent (Lidocaine HCl 2% injection, Huons, Seongnam, Korea). From the local anesthesia stage, the limbs of the rats were spread and fixed to the disinfected surgical plate with a prone position using adhesive tape. A full-thickness flap was elevated, and 7 mm bone defects in diameter were created by bone trephine bur (Osstem Inc., Seoul, Korea). Then, 7 mm diameter bone fragments were removed carefully to avoid tearing dura. The calvaria defects in the Bio-Oss group, the WHHAGs group, and WHHAGs + BMP group were filled with Bio-Oss granules, WHHAGs, and WHHAGs with rhBMP-2, respectively (Fig. 1). Also, the calvaria defects in the NT group remained untreated for 8 weeks. The flap was repositioned and sutured with a synthetic absorbable sterile suture (Coated VICRYL (polyglactin 910), 4 − 0 size) using a simple interrupted suture method.

2.11. Micro-CT Analysis

3D skull images of respective rat groups were obtained using a micro-CT system (Quantum FX micro CT, PerkinElmer, Waltham, USA) to evaluate the regeneration of newly formed bone in the defect site at the moment of 4 and 8 weeks after surgery. The CT scans were obtained at 90 kVp, 108 μA with a field-of-view (FOV) of 20 mm and voxel size of 39 μm. After scanning, a 3D image analysis was conducted using software (Analyze 12.0, AnalyzeDirect Inc., Overland Park, USA) where the region of interest (ROI) was defined as a cylindrical area covering calvarial defect (7.03mm (*d.*) × 2.92mm (*h.*)). Finally, bone volume/tissue volume (BV/TV, %) and bone mineral density (BMD, mg/cm^3) were calculated within the selected ROI.

2.12. Histomorphometry Analysis

Hematoxylin-Eosin (H&E) stain: Four mice from each group were sacrificed, and calvaria bones were isolated for 4 and 8 weeks after surgery. All tissue samples were calcified in 10% ethylenediaminetetraacetic acid (EDTA) (Sigma-Aldrich) for 4 weeks and then embedded in paraffin. Tissue sections (5 μm) were subjected to H&E staining. The post-calcification of calvaria bone tissue was tested by the preclinical center of the Daegu Gyeongbuk Advanced Medical Innovation Foundation (DGMIF).

Masson's trichrome stain: Experiments were performed to observe cells and extracellular matrix related to collagen and bone type in the stained samples. The dyeing process is as follows: A 5 μm-thick paraffin tissue section prepared to observe mineralized and non-mineralized bone tissue according to the degree of collagen production was removed from xylene and immersed in a Bouin solution at room temperature overnight. The tissue samples were rinsed with distilled water several times until the yellow color of the tissue disappeared. After that, nuclear staining was performed in Weigert's iron hematoxylin solution for 10 minutes, washed in running water for 10 minutes, and then stained in Biebrich Scarlet-acid fuchsin solution for 10 minutes. After rinsing several times with distilled water, it was treated in a phosphomolybdic-phosphotungstic acid solution for 10 minutes. After dyeing in Aniline blue solution for 5 minutes, the samples were rinsed several times with distilled water, applied 1% acetic acid solution for 1 to 3 minutes, and then rinsed several times with distilled water. Finally, it was sealed through dehydration and transparent processes. The post-calcification of calvaria bone tissue was tested by the preclinical center of DGMIF

2.13. Statistical Analysis

All of the measurements were statistically analyzed using a statistical program (SPSS 14.0, SPSS Inc., Chicago, USA). The differences in the BV/TV ratio and BMD were analyzed utilizing Student's t-test with $P < 0.05$ being considered significant.

3. Results and discussion

3.1. Characterization of the synthesized WH.

The WH NPs synthesized via the novel wet precipitation method were characterized using XRD, SEM, TEM, and high-resolution TEM images (HRTEM). In Fig. 1A, the XRD pattern of the as-synthesized WH demonstrated that a WH phase with high crystallinity of 93.81% was produced. As shown in Fig. 1B, 1C, the WH NPs show a rhombohedral morphology with a size of ~ 100 nm. The HRTEM image (Fig. 1D) of WH NPs shows a clear lattice spacing of 5.17 Å, corresponding to (110) planes of WH. The fast Fourier transformation (FFT) patterns (Fig. 1E) present that the WH nanocrystal is single crystalline and consistent with the diffraction pattern from the [001] zone axis of the WH rhombohedral phase. Combining scanning transmission electron microscopy (STEM) with element mapping images (Fig. 1G), it was possible to distinguish the component elements, including Mg, Ca, and P with uniform distribution.

The energy dispersive spectroscopy (EDS) analysis (Fig. 1F) shows the distinct peaks of Mg, Ca, and P. The atomic ratio (%) of Mg : Ca : P is 5 : 56 : 39 is close to the theoretical ratio, 5.9 : 52.9 : 41.2. Note that this synthesis method is environmental and biomedical friendly without organic chemicals and acid precursors and scalable synthesis is achieved up to 16 g in a 1 L reactor. (**Figure S1**.)

3.2 Fabrication and characterization of WHHAGs

The thermal stability of the WH NPs obtained prior to the preparation of WHHAGs was investigated. The FTIR (Fig. 2A) and XRD (Fig. 2B) analyses were conducted to characterize the properties of the sintered WH NPs. After sintering treatment at ≤ 700 ºC, (*aka*., WH700), the P-(OH) stretching mode peak at 915 cm^{-1} was maintained, while the P-(OH) peak of samples sintered at 800 ℃ and 1100 ℃ disappeared totally, resulting from the loss of HPO_4^{2-} during the heating treatment. In addition, XRD analysis shows that the peak position of WH700 is obviously different from that of non-sintering WH. However, after heating treatment at 800 ℃, the XRD peaks show an apparent right shit at 0.08 degree. This phenomenon may be explained by the lattice contraction induced by the loss of HPO_4^{2-} according to Bragg's law when samples are sintered at high temperatures above 800 ℃[17, 37]. In this result, 700°C was selected to treat WH/PVA/HAG. Note that HAG is one of the popular commercial products with good osteoconduction and high porosity in dental and orthopedic treatment (Fig. 2C-E). As the second most abundant bone mineral, WH stimulates osteogenic differentiation, inhibits osteoclast activity, and may recapitulate the initial phase of bone regeneration, transitioning to the HAP phase in the early stage of bone regeneration[35, 42]. To achieve the early osteoinductive function of WH, we modified the HAG surface using WH NPs. In our experiments, the synthesized WH was coated on the HAG surface via the assistance of electrostatic interaction of biocompatible polymer and appropriate sintering to remove organic substances, as shown in Scheme 1. As HAG was immersed into WH-PVA solution and dried at 60 ℃, a uniform WH/PVA layer was coated on the HAGs (Figure S2), repeated at least 3 times to obtain a thick layer of WH (Fig. 2F-H). A consequent sintering process of the WH/PVA/HAGs at 700 ℃ for 2 h was carried out to remove PVA and to enhance the bonding strength between the WH layer and HAG. The SEM images of Fig. 2I-K confirmed that the WH NPs were uniformly coated on the surface of HAG. The careful observation using SEM (**Figure S3**) shows that WH NPs were agglomerated to form an interconnected macroporous structure, which is attributed to the recrystallization during the heating treatment and can facilitate the movement of body fluids and nutrients during the healing process of bone defects[43],[44].

3.3 Cells proliferation and regulation of cell cycle

The MG63 cells proliferation assay by CCK-8 is shown in Fig. 3A, where at each time point of 24, 48, and 72 h, the WHHAG50 group showed more significant cell growth than the other groups. All groups are in $P < 0.05$ except for additional indication. The cell proliferation of the WHHAG50 group was about 1.15-, 1.13-, and 1.15- fold higher than that of the NT group at 24 h, 48 h, and 72h, respectively.

To investigate whether stimulation of WHHAGs on the proliferation of the MG63 cells can affect the regulation of the cell cycle, the number of cells at each stage of the cell cycle was measured in MG63 cells after treatment with WHHAGs (Fig. 3B). The number in the S phase was significantly increased in

three WHHAGs treated groups compared to the NT group (Fig. 3C). Also, a similar pattern was observed in the G2/M phase of the cell cycle (Fig. 3D). These results suggest that WHHAGs treatment can stimulate the S and G2/M phases in the cell cycle of MG63 cells. ALP is considered as a marker of early osteogenesis differentiation[38]. To examine the differentiation capacity of WHHAGs, the ALP staining was performed. As shown in **Figure S4**, more intense ALP activity was found in the WHHAG50 group than in the NT group at 14 days. The results clearly indicate that WHHAG50 induced osteogenic differentiation.

3.4. Regulation in downstream signaling pathway of BMP and WNT receptors

Previous studies have reported that BMP2 and canonical WNT signaling pathway can regulate the osteogenic differentiation process in target cells, during which the expression level and function activity of key molecules in one signaling pathway are regulated by the other[45]. The regulatory factors for downstream signaling of BMP and WNT receptors were analyzed in MG63 cells after treatment with WHHAGs to investigate the molecular mechanism of the osteogenic differentiation effects of WHHAGs through a western blot test (Fig. 4A). The expression level of β-catenin (Fig. 4B) and Smad4 (Fig. 4C) proteins were remarkably enhanced in three WHHAGs treated groups compared to the NT group, although dose-dependent increases are observed only in β-catenin. However, the members of the mitogen-activated protein kinase (MAPK) signaling pathway showed different protein expression patterns. The phosphorylation levels of p38 were lower in the WHHAG25 and WHHAG50 treated group than in NT treated group (Fig. 4F), while the phosphorylation levels of signal-regulated kinases (ERKs) and c-Jun N-terminal kinases (JNKs) remained as constant level (Fig. 4D, 4E).

Furthermore, alterations on the expression level of β-catenin and Smad4 proteins were successfully reflected in the expression level of osteogenic genes, including OCN, ALP, RUNX2, BMP2, Col-I, and VEGFA. Significantly increased transcription levels of all genes were detected after the treatment of WHHAGs, although the most significant enhancement was observed in the level of VEGFA (Fig. 5). Therefore, the results suggest that The promotion of WHHAG on the differentiation of MG63 cells is associate with the transcriptional promotion of osteogenic genes in the downstream signaling pathway of BMP and WNT receptors, as depicted in Fig. 6.

Meanwhile, the osteogenic genes used in this study were widely applied as markers for bone cell proliferation because their expression remarkably enhanced during the proliferation of osteoblasts after some stimulators, such as growth factors and natural products[46, 47]. Furthermore, significant alterations on the transcriptional regulation of osteogenic genes were detected in MG63 cells after treatment of several WHHAGs. It is known that the expressions of ALP, COL-I, OCN, and osteoprotegerin (OPG) were decreased generally applied in orthopaedic implants, while the expressions of Runx2 and receptor activator of nuclear factor kappa-B ligand (RANKL) enhanced in the same condition[48]. However, the treatment of ultra-high molecular weight polyethylene (UHMWPE) particles and the

neurotransmitter alpha-calcitonin gene-related peptide (CGRP) for 72 h induced the up-regulation of RANKL and OPG mRNA level in MG63 cells[49].

3.5. Histological Analysis

Histological analyses using H&E and Masson's trichrome staining kits were carefully performed (Fig. 7). The defect sites were identified, and new bone was stained in eosin (Fig. 7A). At 4 weeks after surgery, the calvarial defects filled with fibrous tissue were easily identified in the NT group. As shown in Fig. 7A, the WHHAGs + BMP group showed the early osteogenic bone formation of the same thickness as that of the original bone at the margin of the calvarial defect and irregular-shaped small islets of bone formation. In the Bio-Oss group and the WHHAGs group, osteogenic woven / lamellar bone formation was mostly limited to the defect margin, and the defect gap was filled with granules and fibrous tissue. On the other hand, at 8 weeks after surgery, the formation of new bone was observed in the experimental and control group. However, the healing pattern of the WHHAGs + BMP group was different from that of the NT group. The WHHAGs + BMP group showed more advanced calcification of bone islets near the margin of the calvarial defect and more substantial engagement with the WHHAGs. In the Bio-Oss and WHHAGs groups, more osteogenic woven/lamellar bone formation was observed from the defect margin to the defect center. The WHHAGs group also showed substantial engagement with the WHHAGs. Instead, the Bio-Oss granules do not undergo a healing process and remain intact in the fibrovascular tissue.

The Masson's trichrome staining revealed the degree of new bone mineralization. The red staining indicates mature bone, while the blue staining indicates collagen fiber or regenerated bone (Fig. 7B). The Bio-Oss and WHHAGs groups showed a pale blue color in the center of the defect at the 4th week. However, most of the granules were absorbed in the WHHAGs group compared to the Bio-Oss group, indicating WHHAGs have higher osteogenesis. The WHHAGs + BMP group presented newly formed bone with the same thickness as the original bone, and a dark blue color occurred in the center of the defect, indicating that bone regeneration is actively progressing 4 weeks after surgery. A small amount of mature bone with red dye was observed near the defect margin in the Bio-Oss and WHHAGs groups at 8 weeks after surgery. On the other hand, some mature bones with red dye and initial bones with dark blue dye from the defect margin to the defect center were mixed and evenly observed in the WHHAGs + BMP group at 8 weeks after surgery while maintaining the same thickness as the original bone. Consequently, the potent osteogenic activities of WHHAGs combined with BMP guaranteed granules with excellent outcomes for bone defect repair.

3.6. Micro-CT Analysis

Micro-CT tomographic analysis was carried out to identify bone regeneration (Fig. 7A). Significant bone regeneration was evident in the WHHAGs + BMP group; At the 8-week time point, the calvarial defect displayed almost complete closure with newly formed bone tissue showing higher density than others. Bone regeneration at the 4-week (Fig. 7B), as measured by the BV/TV, was significantly higher in the WHHAGs + BMP group (37.15 ± 8.30%) compared with the NT group (3.06 ± 1.39%; $P < 0.01$) and the Bio-Oss group (11.55 ± 4.12%; $P < 0.01$). By the 8-week timepoint (Fig. 8B), the BV/TV increased in all four

experimental groups with the 4-week timepoint. The results obtained showed a significantly greater BV/TV ratio in the WHHAGs + BMP group (46.27 ± 10.30%) compared with the NT group (6.32 ± 3.87%, $P < 0.01$), the Bio-Oss group (15.70 ± 6.15%, $P < 0.01$) and the WHHAGs group (22.55 ± 1.97%, $P < 0.01$). Moreover, there is significantly greater BV/TV in the WHHAGs group (22.55 ± 1.97%, $P < 0.01$) compared with the NT group (6.32 ± 3.87%, $P < 0.01$). Figure 8C presents bone mineral density (BMD) at the 4-week timepoint where the WHHAGs group (1343.02 ± 20.96 mg/cm^3) was significantly higher than the NT group (1162 ± 5.45 mg/cm^3; $P < 0.05$) and the Bio-Oss group (1193 ± 28.32 mg/cm^3; $P < 0.05$). Also, there is significantly greater BMD in the WHHAGs + BMP (1369.57 ± 27.23 mg/cm^3) compared with the NT group ($P < 0.05$) and the Bio-Oss group ($P < 0.05$). At the 8-week timepoint, BMD was significantly higher in the WHHAGs group (1447.06 ± 24.31 mg/cm^3) compared with the NT group (1215 ± 21.88 mg/cm^3; $P < 0.05$) and the Bio-Oss group (1184 ± 7.68 mg/cm^3; $P < 0.01$). Also, there is significantly greater BMD in the WHHAGs + BMP (1501.49 ± 17.76 mg/cm^3) compared with the NT group ($P < 0.05$) and the Bio-Oss group ($P < 0.01$). The Micro-CT results further confirmed that WHHAGs have a stronger effect on bone regeneration and suggested that the WHHAGs + BMP system is a promising bone substitute in clinical applications.

4. Discussion

As biocompatible biomaterials, HA and WH have different physiochemical properties. WH has better osteogenic ability than HA owing to its magnesium ion release[17, 34, 35]. The Mg^{2+} and PO_4^{3-} released from WH could enhance osteogenesis via the extracellular signal-regulated kinase (ERK) pathway of human turbinate-derived mesenchymal stem cells (hTMSCs) [35]. It has recently been reported that osteogenic ability was increased when HA and WH were presented at proportions present in human bone[50]. WH NPs with rhombohedral morphology and good crystallinity were synthesized via wet precipitation. And scalable synthesis could be easily achieved with this protocol. Compared with previous research, this method is more environmental and biomedical friendly without organic chemicals and acid precursors[42, 56]. BMPs, osteoinductive components of human bone, improve the capability of bone regeneration[51]. Several studies reported that using calcium phosphate as a carrier of BMPs is effective in bone regeneration by taking advantage of the outstanding osteoconductive properties of calcium phosphate[31, 52–54]. In this study, the remarkable features of HAG are its interconnected open porous structure, which is favorable to the in-growth of blood vessels for supplying nutrients to the osteoclast cells and newly formed bone[55]. ALP is considered a relative early marker of osteoblast differentiation, and more intense ALP activity was found in the WHHAG50 group than in the NT group at 14 days, in which WH regulates the early-stage osteogenesis. Owing to the above factors, WHHAGs were constructed to enhance bone formation in the early period of defect healing. WH macroporous layer was coated on the surface of HA granules with dipping and sintering treatment. The formed microporous structure facilitated the exchange of nutrients and wastes for cell growth and biomineralization activity[44].

After osteoblasts have undergone osteogenic differentiation of bone marrow mesenchymal stem cells, the final formation of bone regeneration needs to go through the stages of osteoblast proliferation,

apoptosis, cell migration and adhesion, extracellular matrix maturation, and extracellular matrix mineralization[56]. WHHAG showed the considerable capacity to enhance the proliferation of MG63 by stimulating the S and G2/M phases in the cell cycle. Studies have shown that Mg^{2+} enters osteoblasts through MagT1 and TRPM7 ion channels to promote osteoblast proliferation[56, 57]. The mechanism of WHHAGs to accelerate the osteogenic differentiation was revealed to mediate by activating the downstream signaling pathways of BMP and WNT receptors and up-regulating the transcription level of osteogenic genes (OCN, ALP, Runx2, BMP2, Col , and VEGFA).

In this sense, we attempted to answer the question of how a compound of WH and HA works in bone defects with/without BMP. First WHHAGs were prepared to graft these materials with/without BMPs in rat calvarial defect. Also, this study aimed to clarify whether WHHAGs may possess bone regeneration potential comparable to that of Bio-Oss granules under comparable healing regions in rat calvarial defects. The micro-CT analysis directly showed that WHHAGs accelerated bone remodeling, with the significant increase in newly formed bone tissue, indicating the great osteogenesis and osteointegration activity of WHHAGs. The histological study confirmed that when WHHAGs were applied to calvarial defects, new bone was regenerated without inflammatory reaction. In addition, with the hybridization of BMP with the WHHAGs, bone regeneration potential was superior to the only granules.

5. Conclusions

We developed a scalable synthesis of WH nanocrystals via a wet precipitation method and prepared WHHAGs using a simple dipping and sintering method. The resulting scaffolds exhibited good biocompatibility *in vitro* and enhanced the proliferation of MG63 cells by stimulation of the S and G2/M phases in the cell cycle. WHHAGs stimulate the transcription of osteogenic genes through the regulation of the downstream signaling pathway of BMP and WNT receptors. Particularly, the presence of WH on the surface of HAGs provides stimuli that promote bone regeneration and repair, comparable to that of Bio-Oss granules. Furthermore, bone regeneration was more apparent when BMPs were added to WHHAGs. This study demonstrates that WHHAGs could be useful for bone grafts in clinical areas because WHHAGs have a high potential in the early stage of bone regeneration.

Declarations

Supplementary Information

The online version contains supplementary material available at***

Additional file 1: Table S1. List of antibodies for western blot analyses. **Table S2.** Primer sequences for RT-PCR analyses. **Figure S1.** Dry weight of scalable synthesized WH NPs in 1L batch. **Figure S2.** SEM image of HA granule (C-E), WH/PVA/HA granule (F-H), and WH/HA granule (I-K) with different resolution (1 time dipping). **Figure S3.** SEM images of WHHAGs (3 times dipping). **Figure S4.** Effect of WHHAG on

osteogenic differentiation. ALP staining of NT group and WHHAG50 group after MG63 cell cultured for 7 and 14 days (the scale bar is 100 μm).

Acknowledgement

Not applicable

Authors' contributions

W-BL and CW designed the project and drafted the manuscript; CW performed the materials part experiment, K-JJ and HK provided help with sample characterization; AS, ESP, and DYH implemented and analyzed the cell experiments; W-BL and Y-SJ performed and analyzed the *in vivo* experiments. H-JL made some valuable suggestions for the manuscript. JL and D-SH supervised the whole process of the study. All authors read and approved the final manuscript.

Funding

This work was supported by the National Research Foundation (NRF) of Korea and grants funded by the Ministry of Science, ICT, and Future Planning (MSIP) of Korea (NRF-2019R1A2C2007825).

Availability of data and materials

All data associated with this study are presented in the paper or the Supplementary information. All relevant data are available from the authors.

Competing interests

The authors declare no competing financial interest.

Ethics approval and consent to participate

All animal experimental protocols adhered to the guidelines of Pusan National University Institutional Animal Care and Use Committee (PNUIACUC, South Korea), which comply with the regulation of the International Association for Study of Pain (IASP) in animals. (PNU-2020-2616) .

Consent for publication

Not applicable.

Competing interests

The authors declare no competing interests.

Author details

[1] Department of Oral and Maxillofacial Surgery, Dental and Life Science Institute, School of Dentistry, Pusan National University, Yangsan, 50612, Republic of Korea

[2] Department of Chemistry, Chungnam National University, Daejeon, 34134, Republic of Korea

[3] CAS Key Laboratory for Biomedical Effects of Nanomaterials and Nanosafety, CAS Center for Excellence in Nanoscience, National Center for Nanoscience and Technology of China, Beijing, 100190, China

[4] Department of Biomaterials Science (BK21 FOUR Program)/Life and Industry Convergence Research Institute, College of Natural Resources and Life Science, Pusan National University, Miryang 50463, Korea

[5] Department of Orthopedic Surgery, College of Medicine, Chungnam National University, Daejeon, 35015, Republic of Korea

[6] Dental Research Institute, Pusan National University Dental Hospital, Yangsan, 50612, Republic of Korea

References

1. Coots BK. Alveolar bone grafting: past, present, and new horizons. In: *Seminars in plastic surgery: 2012*. Thieme Medical Publishers: 178–83.
2. Budtz-Jørgensen E, Chung J-P, Rapin C-H. Nutrition and oral health. Best Pract Res Clin Gastroenterol. 2001;15(6):885–96.
3. Mericske-Stern R. Prosthetic considerations. Aust Dent J. 2008;53:49–S59.
4. Gazdag AR, Lane JM, Glaser D, Forster RA. Alternatives to Autogenous Bone Graft: Efficacy and Indications. J Am Acad Orthop Surg. 1995;3(1):1–8.
5. Molly L, Vandromme H, Quirynen M, Schepers E, Adams JL, van Steenberghe D. Bone formation following implantation of bone biomaterials into extraction sites. J Periodontol. 2008;79(6):1108–15.
6. Vaccaro AR. The role of the osteoconductive scaffold in synthetic bone graft. Orthopedics. 2002;25(5 Suppl):571–8.
7. Kim DM, Nevins ML, Lin Z, Fateh A, Kim SW, Schupbach P, Nevins M. The clinical and histologic outcome of dental implant in large ridge defect regenerated with alloplast: a randomized controlled preclinical trial. J Oral Implantol. 2013;39(2):148–53.
8. Muller P, Bulnheim U, Diener A, Luthen F, Teller M, Klinkenberg ED, Neumann HG, Nebe B, Liebold A, Steinhoff G, et al. Calcium phosphate surfaces promote osteogenic differentiation of mesenchymal stem cells. J Cell Mol Med. 2008;12(1):281–91.
9. Shih YR, Hwang Y, Phadke A, Kang H, Hwang NS, Caro EJ, Nguyen S, Siu M, Theodorakis EA, Gianneschi NC, et al. Calcium phosphate-bearing matrices induce osteogenic differentiation of stem

cells through adenosine signaling. Proc Natl Acad Sci U S A. 2014;111(3):990–5.

10. Jeong KJ, Song Y, Shin HR, Kim JE, Kim J, Sun F, Hwang DY, Lee J. In vivo study on the biocompatibility of chitosan–hydroxyapatite film depending on degree of deacetylation. J Biomedical Mater Res Part A. 2017;105(6):1637–45.
11. Wang C, Ma Z, Yuan K, Ji T. Using scaffolds as drug delivery systems to treat bone tumor. Nanotechnology. 2022;33(21):212002.
12. Choi S-W, Kang J, Wang C, Lee HM, Oh S-J, Pak K, Shin N, Lee I-W, Lee J, Kong S-K. Human tonsil-derived mesenchymal stem cells-loaded hydroxyapatite-chitosan patch for mastoid obliteration. ACS Appl Bio Mater. 2020;3(2):1008–17.
13. Yoshikawa H, Myoui A. Bone tissue engineering with porous hydroxyapatite ceramics. J Artif Organs. 2005;8(3):131–6.
14. Samavedi S, Whittington AR, Goldstein AS. Calcium phosphate ceramics in bone tissue engineering: a review of properties and their influence on cell behavior. Acta Biomater. 2013;9(9):8037–45.
15. Patel N, Best SM, Bonfield W, Gibson IR, Hing KA, Damien E, Revell PA. A comparative study on the in vivo behavior of hydroxyapatite and silicon substituted hydroxyapatite granules. J Mater Sci Mater Med. 2002;13(12):1199–206.
16. Lim JY, Donahue HJ. Cell sensing and response to micro- and nanostructured surfaces produced by chemical and topographic patterning. Tissue Eng. 2007;13(8):1879–91.
17. Jang HL, Jin K, Lee J, Kim Y, Nahm SH, Hong KS, Nam KT. Revisiting whitlockite, the second most abundant biomineral in bone: nanocrystal synthesis in physiologically relevant conditions and biocompatibility evaluation. ACS Nano. 2014;8(1):634–41.
18. Hong KS, Nam KT, Jang HL, Ryu HS, Jin KS. Whitlockite and method for manufacturing the same. In.: Google Patents; 2015.
19. Chang BS, Lee CK, Hong KS, Youn HJ, Ryu HS, Chung SS, Park KW. Osteoconduction at porous hydroxyapatite with various pore configurations. Biomaterials. 2000;21(12):1291–8.
20. Chen L, Jiang W, Huang J, He BC, Zuo GW, Zhang W, Luo Q, Shi Q, Zhang BQ, Wagner ER, et al. Insulin-like growth factor 2 (IGF-2) potentiates BMP-9-induced osteogenic differentiation and bone formation. J Bone Miner Res. 2010;25(11):2447–59.
21. Groeneveld EH, Burger EH. Bone morphogenetic proteins in human bone regeneration. Eur J Endocrinol. 2000;142(1):9–21.
22. Zhao J, Shinkai M, Takezawa T, Ohba S, Chung UI, Nagamune T. Bone regeneration using collagen type I vitrigel with bone morphogenetic protein-2. J Biosci Bioeng. 2009;107(3):318–23.
23. Friedlaender GE, Perry CR, Cole JD, Cook SD, Cierny G, Muschler GF, Zych GA, Calhoun JH, LaForte AJ, Yin S. Osteogenic protein-1 (bone morphogenetic protein-7) in the treatment of tibial nonunions. J Bone Joint Surg Am. Suppl 2001;1(Pt 2):83–A.
24. Glass DA, Mellonig JT, Towle HJ. Histologic evaluation of bone inductive proteins complexed with coralline hydroxylapatite in an extraskeletal site of the rat. J Periodontol. 1989;60(3):121–6.

25. Miller TA, Ishida K, Kobayashi M, Wollman JS, Turk AE, Holmes RE. The induction of bone by an osteogenic protein and the conduction of bone by porous hydroxyapatite: a laboratory study in the rabbit. Plast Reconstr Surg. 1991;87(1):87–95.
26. Ripamonti U, Ma SS, van den Heever B, Reddi AH. Osteogenin, a bone morphogenetic protein, adsorbed on porous hydroxyapatite substrata, induces rapid bone differentiation in calvarial defects of adult primates. Plast Reconstr Surg. 1992;90(3):382–93.
27. Urist MR, Kovacs S, Yates KA. Regeneration of an enchondroma defect under the influence of an implant of human bone morphogenetic protein. J Hand Surg Am. 1986;11(3):417–9.
28. Ono I, Ohura T, Murata M, Yamaguchi H, Ohnuma Y, Kuboki Y. A study on bone induction in hydroxyapatite combined with bone morphogenetic protein. Plast Reconstr Surg. 1992;90(5):870–9.
29. Ono I, Gunji H, Kaneko F, Saito T, Kuboki Y. Efficacy of hydroxyapatite ceramic as a carrier for recombinant human bone morphogenetic protein. J Craniofac Surg. 1995;6(3):238–44.
30. Freilich M, C MP, Wei M, Shafer D, Schleier P, Hortschansky P, Kompali R, Kuhn L. Growth of new bone guided by implants in a murine calvarial model. Bone. 2008;43(4):781–8.
31. Alam MI, Asahina I, Ohmamiuda K, Takahashi K, Yokota S, Enomoto S. Evaluation of ceramics composed of different hydroxyapatite to tricalcium phosphate ratios as carriers for rhBMP-2. Biomaterials. 2001;22(12):1643–51.
32. Scotchford CA, Vickers M, Ali SY. The isolation and characterization of magnesium whitlockite crystals from human articular cartilage. Osteoarthritis Cartilage. 1995;3(2):79–94.
33. Jeong J, Kim JH, Shim JH, Hwang NS, Heo CY. Bioactive calcium phosphate materials and applications in bone regeneration. Biomater Res. 2019;23:4.
34. Jang HL, Zheng GB, Park J, Kim HD, Baek HR, Lee HK, Lee K, Han HN, Lee CK, Hwang NS, et al. In Vitro and In Vivo Evaluation of Whitlockite Biocompatibility: Comparative Study with Hydroxyapatite and beta-Tricalcium Phosphate. Adv Healthc Mater. 2016;5(1):128–36.
35. Kim HD, Jang HL, Ahn HY, Lee HK, Park J, Lee ES, Lee EA, Jeong YH, Kim DG, Nam KT, et al. Biomimetic whitlockite inorganic nanoparticles-mediated in situ remodeling and rapid bone regeneration. Biomaterials. 2017;112:31–43.
36. Kim HK, Han HS, Lee KS, Lee DH, Lee JW, Jeon H, Cho SY, Roh HJ, Kim YC, Seok HK. Comprehensive study on the roles of released ions from biodegradable Mg-5 wt% Ca-1 wt% Zn alloy in bone regeneration. J Tissue Eng Regen Med. 2017;11(10):2710–24.
37. Lee WB, Wang C, Lee JH, Jeong KJ, Jang YS, Park JY, Ryu MH, Kim UK, Lee J, Hwang DS. Whitlockite Granules on Bone Regeneration in Defect of Rat Calvaria. ACS Appl Bio Mater. 2020;3(11):7762–8.
38. Gotman I, Ben-David D, Unger RE, Bose T, Gutmanas EY, Kirkpatrick CJ. Mesenchymal stem cell proliferation and differentiation on load-bearing trabecular Nitinol scaffolds. Acta Biomater. 2013;9(9):8440–8.
39. Yu J, Li W, Tang L, Luo Y, Xu J. In vivo and in vitro effects of chronical exposure to nonylphenol on lipid metabolism. Environ Sci Europe. 2020;32(1):1–12.

40. Chen J, Gong S, Wan X, Gao X, Wang C, Zeng F, Zhao C, Liu B, Huang Y. Hypolipidemic properties of Chlorella pyrenoidosa organic acids via AMPK/HMGCR/SREBP-1c pathway in vivo. Food Sci Nutr. 2021;9(1):459–68.
41. Liu W-w, Meng J, Cui J, Luan Y-s. Characterization and function of microRNA∗ s in plants. Front Plant Sci. 2017;8:2200.
42. Wang C, Jeong K-J, Park HJ, Lee M, Ryu S-C, Hwang DY, Nam KH, Han IH, Lee J. Synthesis and formation mechanism of bone mineral, whitlockite nanocrystals in tri-solvent system. J Colloid Interface Sci. 2020;569:1–11.
43. Ghosh R, Sarkar R. Synthesis and characterization of sintered hydroxyapatite: a comparative study on the effect of preparation route. J Aust Ceram Soc. 2018;54(1):71–80.
44. Jang HL, Lee K, Kang CS, Lee HK, Ahn H-Y, Jeong H-Y, Park S, Kim SC, Jin K, Park J. Biofunctionalized ceramic with self-assembled networks of nanochannels. ACS Nano. 2015;9(4):4447–57.
45. Lin GL, Hankenson KD. Integration of BMP, Wnt, and notch signaling pathways in osteoblast differentiation. J Cell Biochem. 2011;112(12):3491–501.
46. Zhang L, Ai H. Concentrated growth factor promotes proliferation, osteogenic differentiation, and angiogenic potential of rabbit periosteum-derived cells in vitro. J Orthop Surg Res. 2019;14(1):146.
47. Baek M, Seo M, Lee JH, Kim I-W, Kim M, Hwang J-S. Osteoblastogenic activity of Locusta migratoria ethanol extracts on pre-osteoblastic MG-63 cells. J Life Sci. 2018;28(12):1448–54.
48. Xie H, Wang P, Wu J. Effect of exposure of osteoblast-like cells to low-dose silver nanoparticles: uptake, retention and osteogenic activity. Artif Cells Nanomed Biotechnol. 2019;47(1):260–7.
49. Xu J, Kauther MD, Hartl J, Wedemeyer C. Study was performed at the University of Duisburg - Essen G: Effects of alpha-calcitonin gene-related peptide on osteoprotegerin and receptor activator of nuclear factor-kappaB ligand expression in MG-63 osteoblast-like cells exposed to polyethylene particles. J Orthop Surg Res. 2010;5:83.
50. Cheng H, Chabok R, Guan X, Chawla A, Li Y, Khademhosseini A, Jang HL. Synergistic interplay between the two major bone minerals, hydroxyapatite and whitlockite nanoparticles, for osteogenic differentiation of mesenchymal stem cells. Acta Biomater. 2018;69:342–51.
51. Urist MR, Strates BS. Bone morphogenetic protein. J Dent Res. 1971;50(6):1392–406.
52. Gu H, Xue Z, Wang M, Yang M, Wang K, Xu D. Effect of Hydroxyapatite Surface on BMP-2 Biological Properties by Docking and Molecular Simulation Approaches. J Phys Chem B. 2019;123(15):3372–82.
53. Zhou P, Wu J, Xia Y, Yuan Y, Zhang H, Xu S, Lin K. Loading BMP-2 on nanostructured hydroxyapatite microspheres for rapid bone regeneration. Int J Nanomedicine. 2018;13:4083–92.
54. Rohanizadeh R, Chung K. Hydroxyapatite as a carrier for bone morphogenetic protein. J Oral Implantol. 2011;37(6):659–72.
55. Gao P, Zhang H, Liu Y, Fan B, Li X, Xiao X, Lan P, Li M, Geng L, Liu D. Beta-tricalcium phosphate granules improve osteogenesis in vitro and establish innovative osteo-regenerators for bone tissue

engineering in vivo. Sci Rep. 2016;6(1):1–14.

56. Schneider RK, Puellen A, Kramann R, Raupach K, Bornemann J, Knuechel R, Pérez-Bouza A, Neuss S. The osteogenic differentiation of adult bone marrow and perinatal umbilical mesenchymal stem cells and matrix remodelling in three-dimensional collagen scaffolds. Biomaterials. 2010;31(3):467–80.
57. Wang N, Yang S, Shi H, Song Y, Sun H, Wang Q, Tan L, Guo S. Magnesium alloys for orthopedic applications: A review on the mechanisms driving bone healing. J Magnesium Alloys 2022.

Scheme

Scheme 1 is available in the Supplementary Files section.

Figures

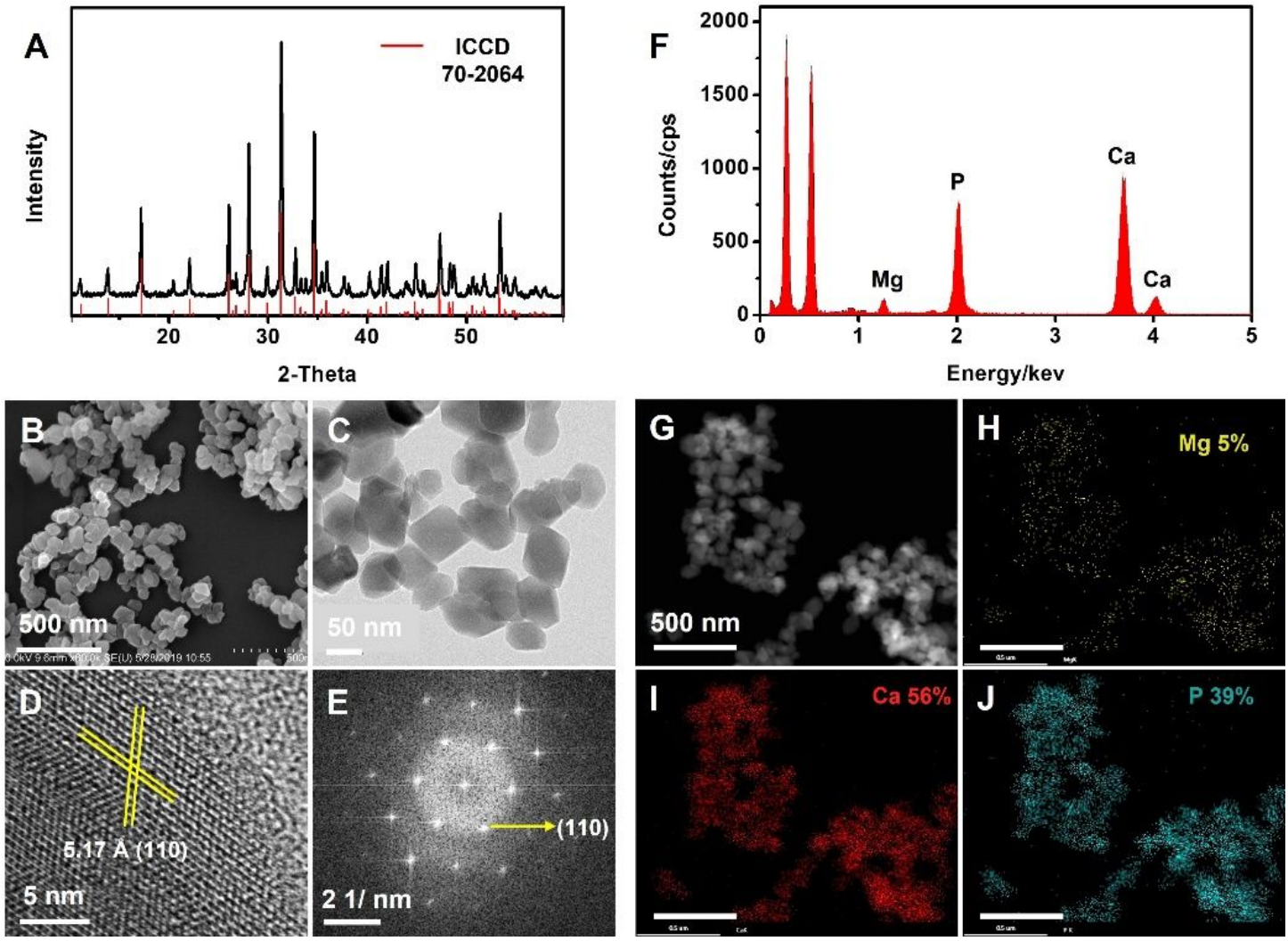

Figure 1

Synthesis and characterization of WH NPs.(A) XRD patterns, (B) SEM, (C) TEM (D) HRTEM, (E) FFT, (F) EDX analysis, (G) HAADF-STEM image, and (H-J) elemental mapping of WH NPs.

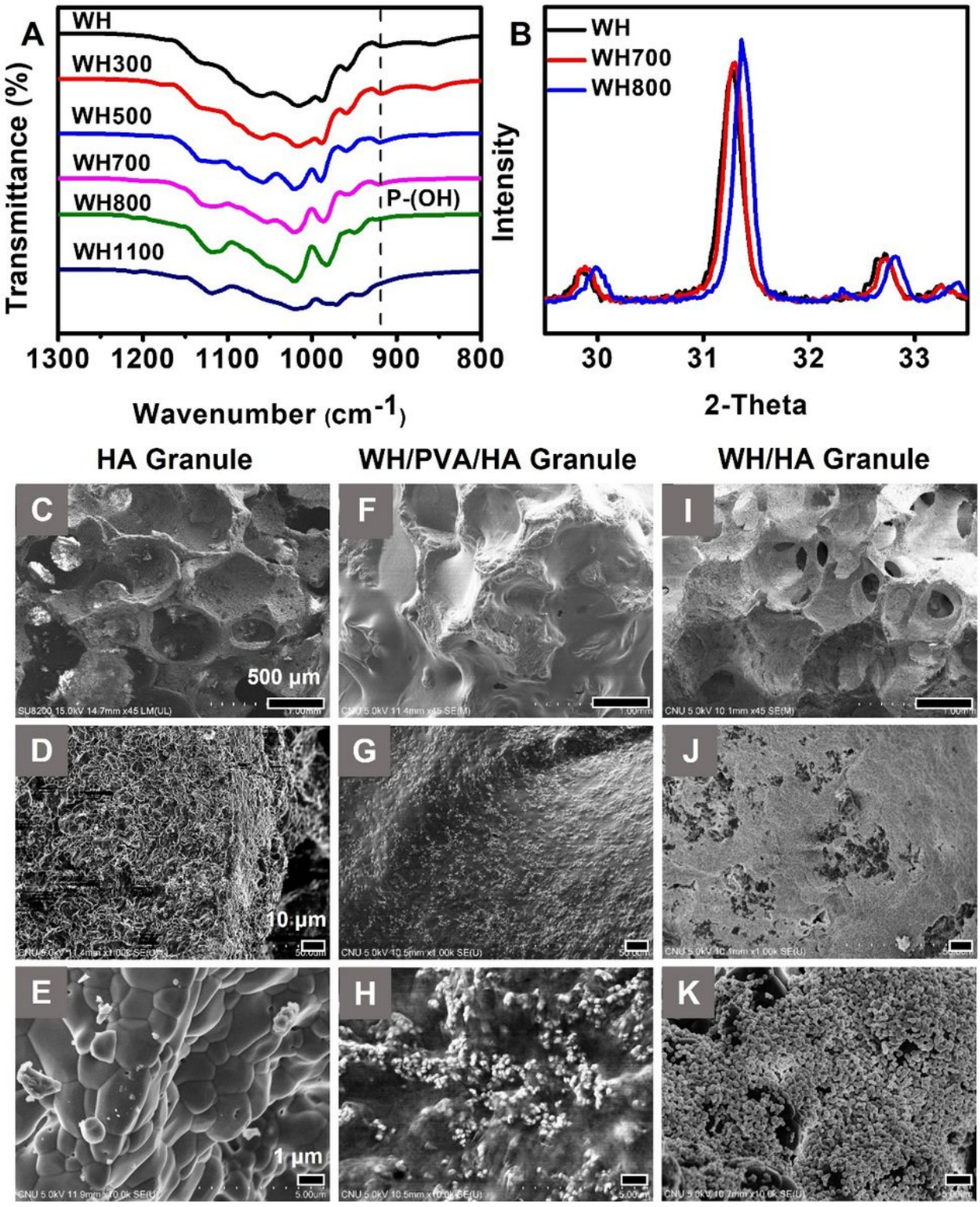

Figure 2

Characterization of sintered WH NPs and WHHAGs. (A) FTIR spectra of WH after sintering treatment with different temperatures. (B) XRD analysis of WH, WH after sintering treatment at 700 and 800 °C. SEM

image of HA granules (C-E), WH/PVA/HA granules (F-H), and WH/HA granules (*aka.,* WHHAGs) (I-K) with different resolutions.

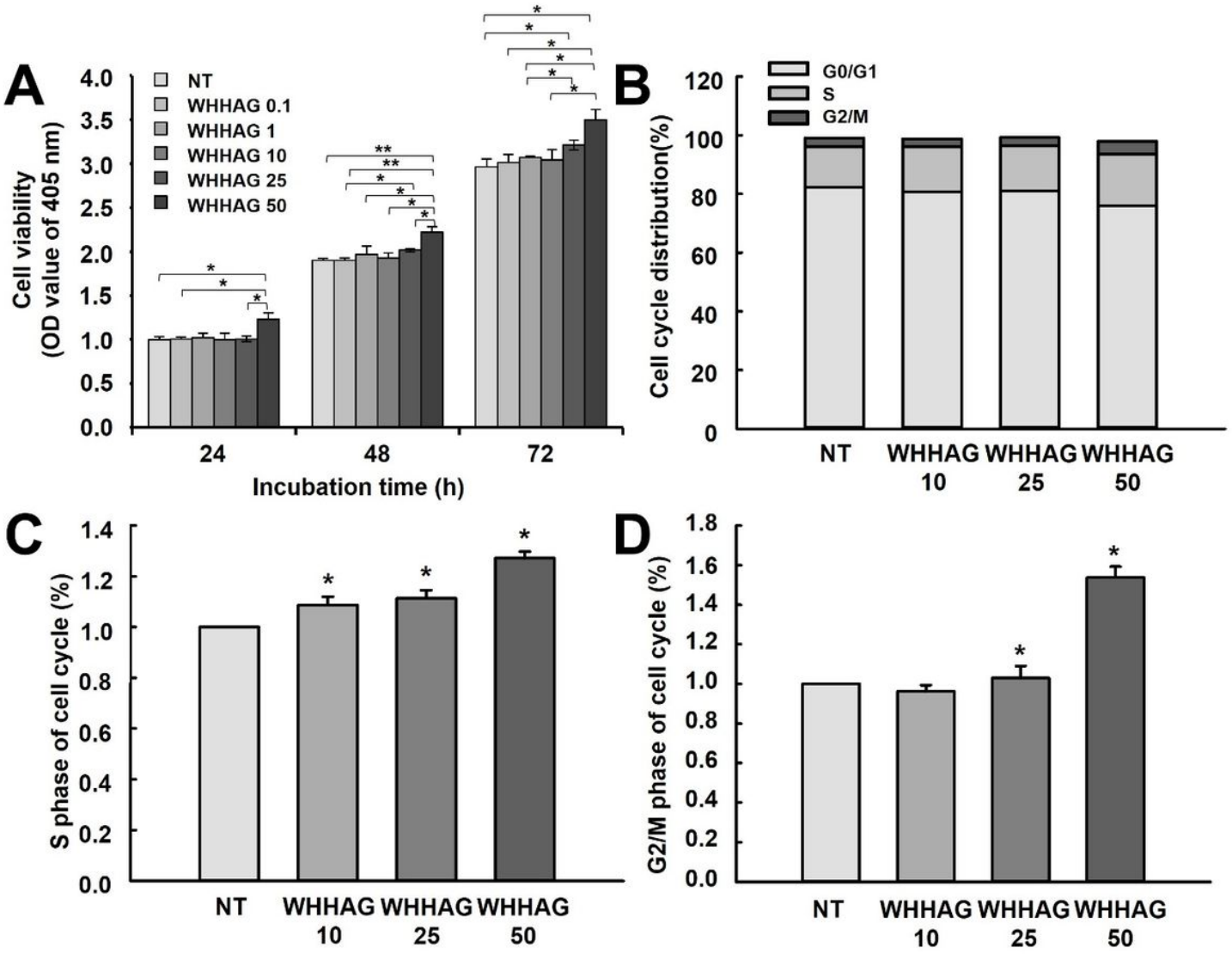

Figure 3

***In vitro* cell tests of WHHAGs.** (A) The MG63 cells proliferation assay by CCK-8.

(B) Cell cycle distribution. The cell cycle distribution of MG63 cells treated with WHHAGs was analyzed with flow cytometric analysis of the DNA content of nuclei of cells after staining with propidium iodide (PI). (C-D) Analysis of cell number % of each cell cycle phase relative to total phases. The number of cells in the S (C) and G2/M (D) stages was determined at each time point, and each phase% was calculated as the percentage of the number of cells in the specific population relative to the number of total cells. The data represent the means ± SD of three replicates. * indsicates $p < 0.05$, ** indicates $p < 0.01$.

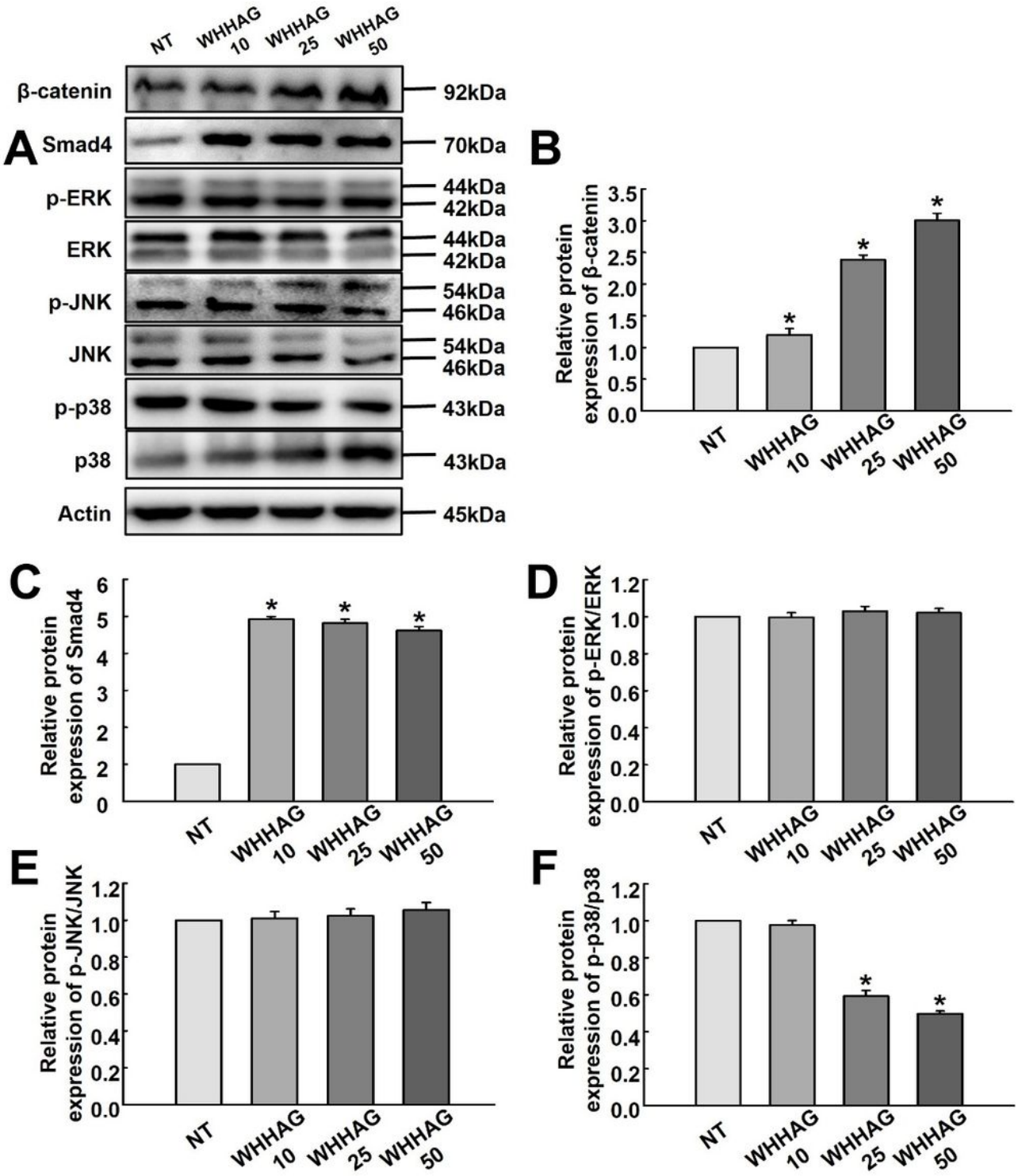

Figure 4

Western blot analyses for regulatory factors in downstream signaling of BMP and WNT receptors. The expression levels of b-catenin, Smad4, p-ERK, ERK, p-JNK, JNK, p-p38, and p38 proteins were determined in MG63 cells treated with WHHAGs for 72 h using specific antibodies. After determining the intensity of each band using an imaging densitometer, the relative levels of each protein were calculated based on

the band intensity of β-actin protein as the endogenous control. The data represent the means ± SD of three replicates. * indicates $p < 0.05$ compared to the untreated group.

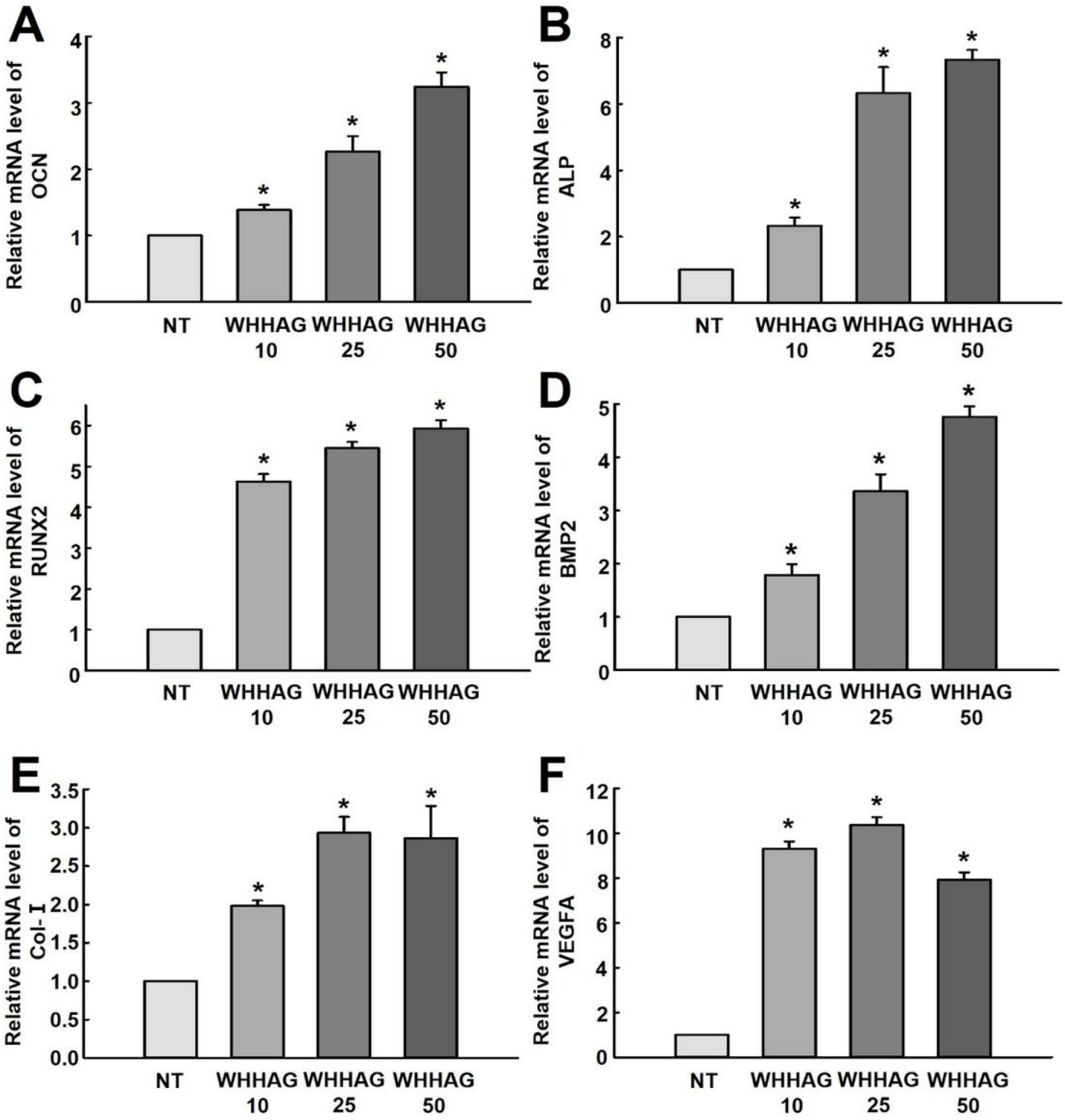

Figure 5

Transcription level of osteogenic genes. After collection of total RNA from MG63 cells treated with WHHAGs for 72 h, the mRNA levels of OCN, ALP, RUNX2, BMP2, Col-I, and VEGFA genes were measured

by RT-qPCR as described in materials and methods. The data represent the means ± SD of duplicates. * indicates $p < 0.05$ compared to the NT group.

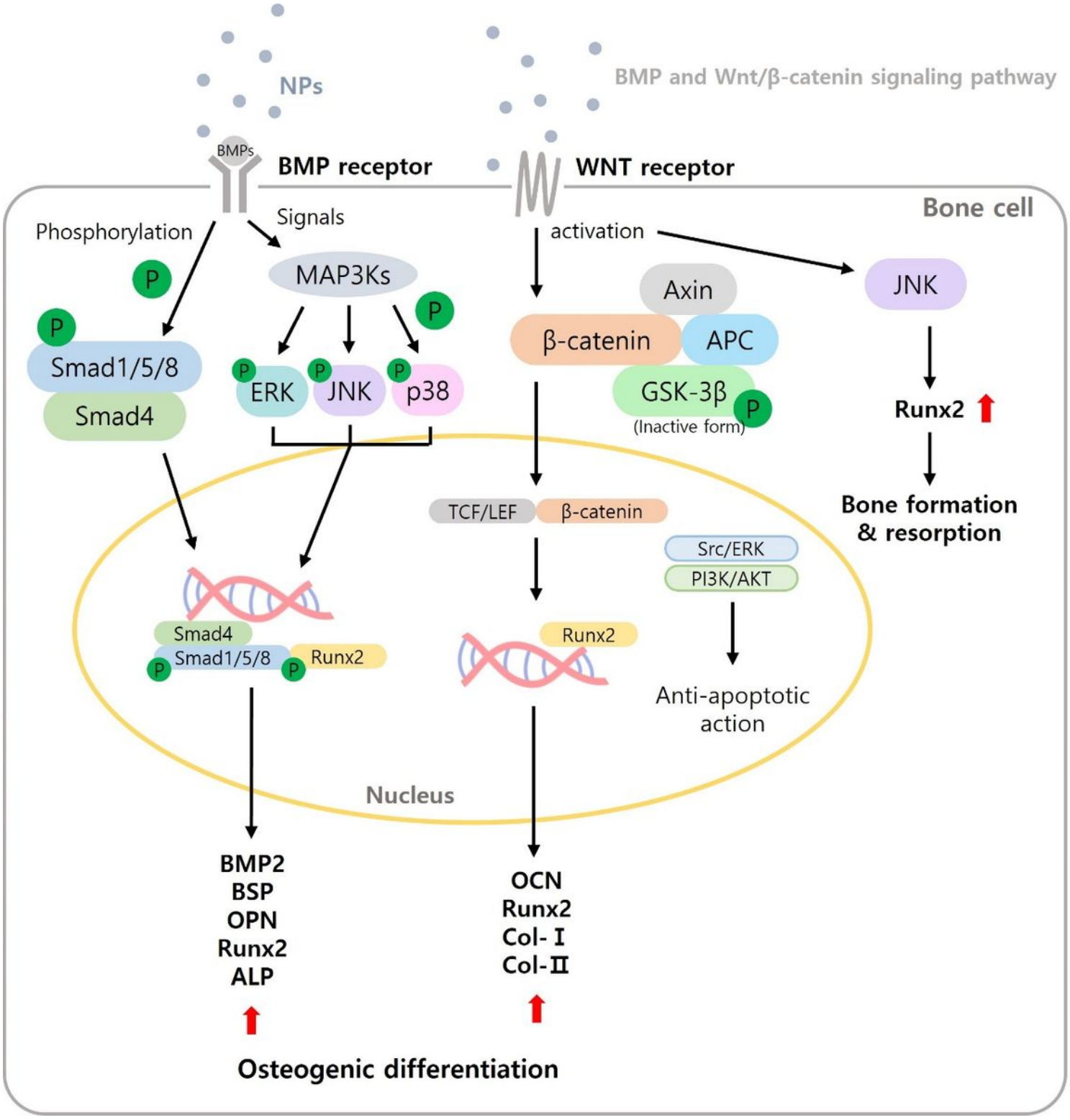

Figure 6

Two conventional osteogenic differentiation pathways of MSCs/preosteoblasts. i.e., the bone morphogenic pathway and the Wnt/β-catenin pathway. MAPK: mitogen-activated protein kinase; Smad:

small mothers against decapentaplegic; ERK: Extracellular signal-regulated kinase; JNK: c-Jun N-terminal kinases; APC: Adenomatous polyposis coli; GSK-3β: Glycogen synthase kinase-3β; PI3K: Phosphatidylinositol 3-kinase; BMP2: Bone Morphogenic Protein 2; BSP: Bone sialoprotein; OPN : Osteopontin; RUNX2: Runt-related transcription factor 2; OCN: Osteocalcin; Col: collagen; ALP: Alkaline phosphatase.

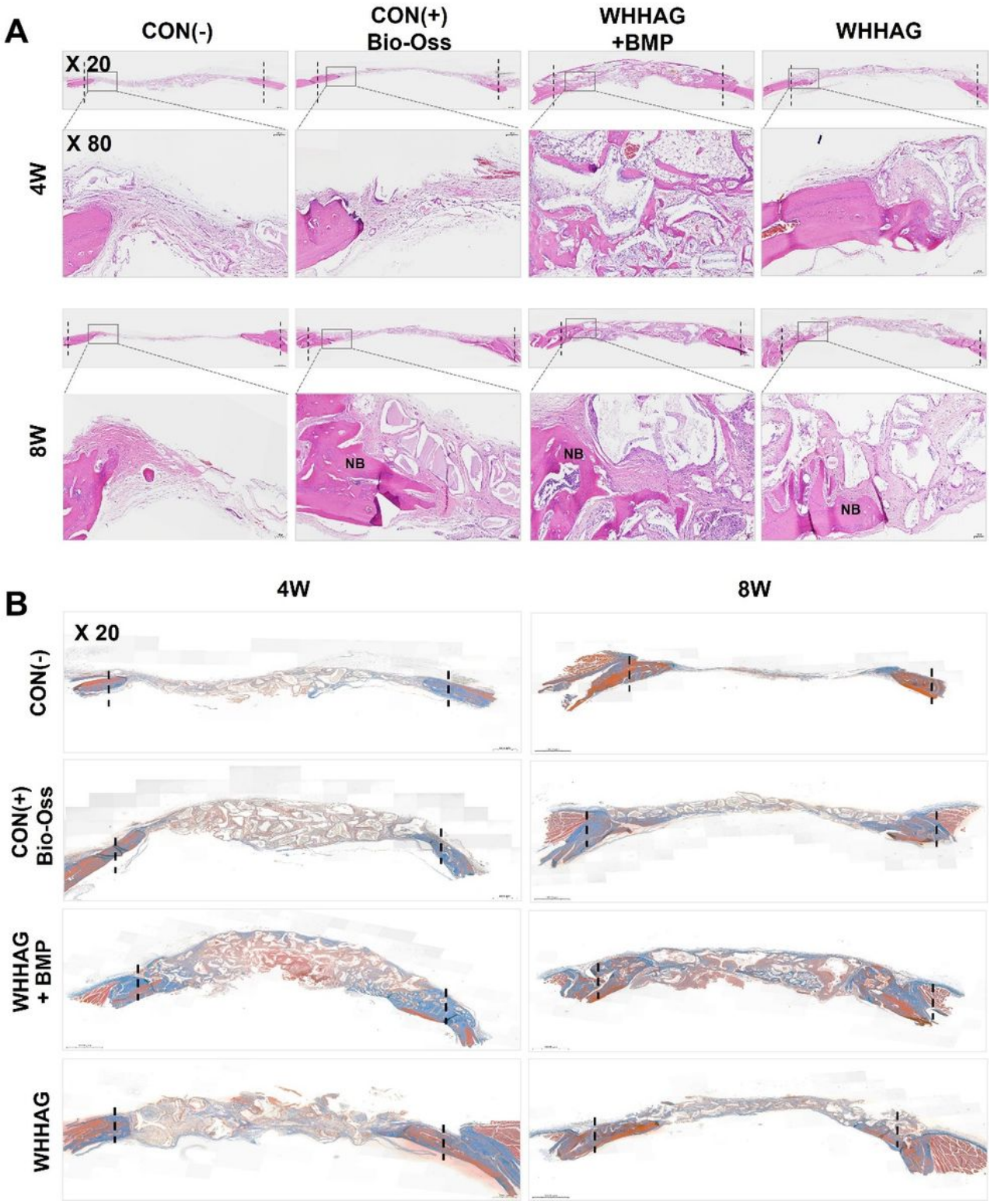

Figure 7

Histological assessment of bone regeneration at 4 weeks and 8 weeks. (A) Coronal plane sections were stained with (A) hematoxylin and eosin (H&E) and (B) Masson's trichrome.

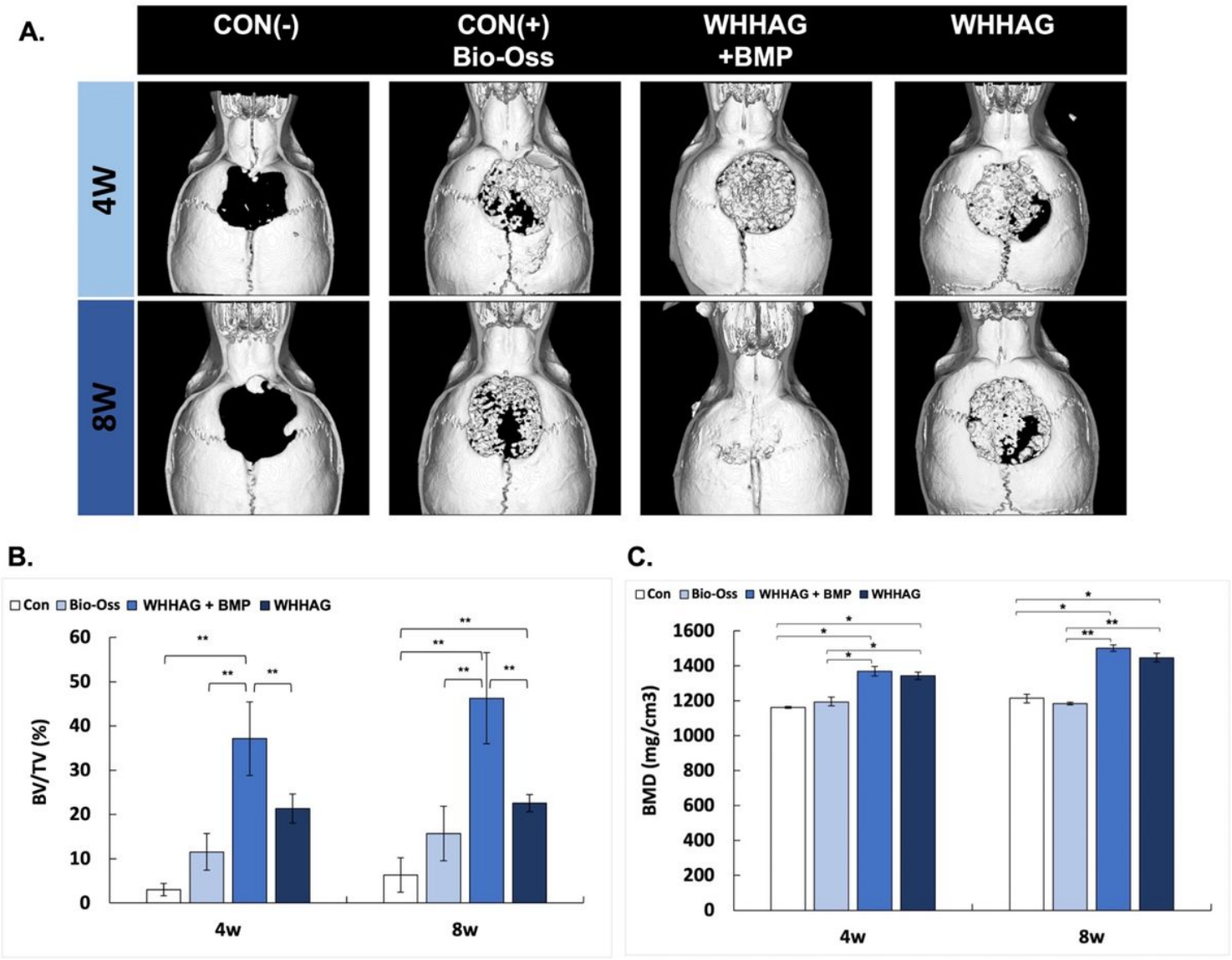

Figure 8

Micro-CT tomographic analysis and bone volume fraction and bone mineral density analyses. (A) Three-dimensional micro-CT horizontal images of rat calvaria at 4 weeks and 8 weeks after surgery. The calvarial defect displayed almost complete closure with newly formed bone tissue showing higher density in the WHHAGs + BMP group at 8 weeks after surgery. (B) Bone volume fraction (BV/TV, %) at 4 and 8 weeks after surgery. (C) Bone mineral density (BMD, mg/cm^3) at 4 and 8 weeks after surgery. * indsicates $p < 0.05$, ** indicates $p < 0.01$ (n=4).

Supplementary Files

This is a list of supplementary files associated with this preprint. Click to download.

- Supportinginformation.docx
- floatimage1.jpeg